Neuromechanical Consequences of Epimuscular Myofascial Force Transmission

Bernabei, M.

2017

5

Longitudinal and transversal displacements between triceps surae muscles during locomotion of the rat

The functional consequences of differential muscle activation and contractile behavior between mechanically coupled synergists are still poorly understood. Even though synergistic muscles exert similar mechanical effects at the joint they span, differences in the anatomy, morphology and neural drive may lead to non-uniform contractile conditions. This study aimed to investigate the patterns of activation and contractile behaviour of triceps surae muscles, to understand how these contribute to the relative displacement between the one-joint soleus (SO) and two-joint lateral gastrocnemius (LG) muscle bellies and their distal tendons during locomotion in the rat.

In seven rats, muscle belly lengths and muscle activation during level and upslope trotting were measured by sonomicrometry crystals and electromyographic electrodes chronically implanted in SO and LG. Length changes of muscle-tendon units (MTUs) and tendon fascicles were estimated based on joints kinematics and muscle bellies lengths. Distances between implanted crystals were further used to assess longitudinal and transversal deformations of the intermuscular volume between SO and LG.

For both slope conditions, we observed differential timing of muscle activation as well as substantial differences in contraction speeds between muscle bellies (maximal relative speed 55.9mm/s). Muscle lengths and velocities did not significantly differ between level and upslope locomotion, only EMG amplitude of LG was affected by slope. Relative displacements between SO and LG MTUs were found in both longitudinal and transversal directions, yielding an estimated maximal length difference of 2.1 mm between their distal tendons. Such relative displacements may have implications for the force exchanged via intermuscular and intertendinous pathways.

Adapted from: Bernabei M, Maas H, van Dieën JH. *Longitudinal and transversal displacements between triceps surae muscles during locomotion of the rat*. J Exp Biol (2016). [accepted]

5.1 Introduction

Animal movement is the result of the interaction and coordination of multiple muscles. Despite the importance of understanding such complex functional integration (Higham and Biewener, 2008), little is known about the consequences of differential fiber strain and level of activation occurring *in vivo* between individual muscles which cooperate within a synergistic muscle group. Regional variation in strain and heterogeneous patterns of activation have been observed between fascicles within muscles and between synergistic muscles during normal movements of the toad, cat, rat, guinea fowl and human (Ahn et al., 2003; English, 1984; Gillis and Biewener, 2001; Higham and Biewener, 2008; Lichtwark et al., 2007; Maas et al., 2009; Wakeling, 2009). Such variation is the result of morphological and architectural differences within and between muscles, such as cross-sectional area, fibre-type composition, pennation angle, activation history, level of fatigue, timing of activation and in series tendon compliance (Higham and Biewener, 2011). These variations in strain may have effects on muscle force production through mechanical interactions between muscles mediated by in series common elasticity (Sandercock, 2000; Tijs et al., 2014a) and myofascial connections (Maas and Sandercock, 2010).

The triceps surae muscles of the rat have been widely used as an experimental model for investigating the mechanical properties of skeletal muscles (Bobbert et al., 1990; Devasahayam and Sandercock, 1992; Ettema and Huijing, 1994; Messner et al., 1999; Pickett et al., 2008). As a consequence, the anatomy, physiology and mechanical properties of these muscles are well characterized. Soleus (SO) and gastrocnemii (GAS; medial and lateral gastrocnemius, MG and LG) muscles share a similar anatomical location and function at the ankle joint, but differ substantially in pennation angle (Close, 1964; Heslinga and Huijing, 1990) and fibre type composition (Armstrong and Phelps, 1984). SO is mainly composed of slow-twitch oxidative fibers (87%), while LG and MG consist mainly of fast-twitch oxidative-glycolytic (28%) or fast-twitch glycolytic (65%) fibers (Armstrong and Phelps, 1984). SO is much smaller than GAS, with a physiological cross-sectional area of 8.8 mm^2 and 63.3 mm^2 for SO and LG, respectively (Woittiez et al., 1985). In contrast to SO, GAS spans also the knee joint. As a consequence, changes in knee joint angle will result in changes GAS length as well as changes in the relative positions of these muscles. Such anatomical and morphological organization can have consequences for muscle mechanics. When manipulating the relative position of muscle-tendon units within a physiological range *in situ*, mechanical interaction between SO and LG was found (Bernabei et al., 2015). Previous studies have investigated the activation and length changes of the triceps surae

muscles *in vivo* (Hodson-Tole and Wakeling, 2007; Hodson-Tole and Wakeling, 2008), yet muscle relative displacements have not been measured.

Displacement between muscle bellies and/or tendons of neighbouring muscles is associated with changes in the transmission of force via intermuscular or intertendinous connective tissues pathways. Changes in muscle relative position of SO and LG are expected due to differential changes in muscle-tendon-unit (MTU) length and differences in contraction velocities of the muscle bellies. Such differences, in turn, can be the result of differential activation levels, asynchronous patterns of activation, differences in pennation angle, or a consequence of joint angle changes as the two neighbouring muscles span different joints and have different moment arms. To date, a number of *in situ* studies have reported mechanical effects of changes in muscle relative position (Huijing, 2009). More recently, ultrasound studies have reported displacements between SO and GAS in humans, but only for passive muscle conditions during isolated knee movements or selective electrical stimulation of targeted muscles at fixed joint angles (Bojsen-Moller et al., 2010; Finni et al., 2015; Oda et al., 2007; Tian et al., 2012). In addition, such relative displacements were measured in one dimension. Therefore, very little is known about the magnitudes of displacement between SO and GAS muscles during normal movements and, hence, physiological motor unit recruitment.

The aim of this study was to investigate the coordinated action of ankle plantar-flexors during locomotion and to analyze how this adapts to varying locomotor demands. In particular, we assessed the patterns of activation and contractile behaviour of triceps surae muscles, as well as the 3D relative displacement between the one-joint SO and the two-joint LG muscle bellies and distal tendons during level and upslope trotting. We expected that during upslope trotting the increased mechanical demands and altered knee joint kinematics would increase the relative displacement between adjacent muscle bellies. We hypothesized that such increased relative displacement would be associated with a substantial increase of differential length changes of both muscles as well as deformation of the tissues connecting them, due to differences in muscle activation patterns, effects of in series compliance and intermuscular connections. These differences may affect the moment produced at the knee and ankle joints and, thus, help understanding how different muscles cooperate to achieve their functional role.

5.2 Methods

5.2.1 Animal care and training

Seven male Wistar rats (*rattus norvegicus*, body mass 277.6 ± 15.7g; 7 weeks old upon arrival) were tested in this study. Before implantation of sensors, each rat was trained to run on a Plexiglas-enclosed, custom-built, motor-driven treadmill (Westra et al., 1985) for 10 days. Food rewards were provided upon completion of the 2 min running task at increasing speed (up to 0.8 m/s) and slope (up to 20°). To promote running, a movable electrical grid placed at the back of the treadmill was used to deliver mild electrical shocks. Before touching the grid, the rats came into contact with a small object. After two days, the rats were trained to avoid the electrical shocks by responding to the object. During training and data collection, rats were housed in large cages (0.55 × 0.33 × 0.20 m) with access to food and water *ad libitum*. All surgical and experimental procedures were approved by the Committee on the Ethics of Animal Experimentation at the Vrije Universiteit Amsterdam (protocol number FBW 12-01) and in strict agreement with the guidelines and regulations concerning animal welfare and experimentation set forth by Dutch law. On completion of measurements, animals were euthanized with a pentobarbital overdose (Euthasol 20%) injected intracardially, followed by double sided pneumothorax.

5.2.2 Sensors implantation

All surgical procedures were performed under aseptic conditions. Rats were anesthetized using isofluorane gas (3% induction, 1.4-2% maintenance). A one-time subcutaneous injection of Buprenorphine (opiate, Temgesic®, Schering-Plough, Maarssen, The Netherlands) at dosage of 0.02 mg/kg was administered pre-operatively. The right hindlimb was surgically instrumented with sonomicrometry crystals and fine-wire electromyography (EMG) electrodes using procedures described previously (Maas et al., 2009). To measure muscle belly lengths and relative positions, two piezoelectric crystals (1mm; Sonometrics, London, ON, Canada) were implanted near the proximal and distal aponeurosis of each muscle (see Fig. 5.1A, colored circles). To measure EMG activity, pairs of Teflon-insulated multistranded stainless steel fine-wire electrodes (25μm un-coated diameter, 7SS-1T, Science products GmbH, Hofheim, Germany) were chronically implanted in the mid-region of SO and LG muscle bellies. Muscle bellies were accessed by opening the skin and the crural fascia from the lateral side. The EMG electrodes were implanted approximately 2mm deep and approximately 1mm apart. A reference electrode was inserted underneath the skin, in the region above the gluteus maximus muscle. Given the distribution of fiber type in

SO and LG muscle regions (Armstrong and Phelps, 1984) and muscle architecture (Prodanov et al., 2005), the EMG pick-up area consisted of slow oxidative fibers in the SO and a majority of fast glycolytic fibers in the LG. Electrode placement was verified by stimulation through the implanted wires. In addition, pictures of the implant were taken on the euthanized animal after data collection to verify consistent positioning and to exclude dislodging of EMG electrodes and sonomicrometry crystals.

Two other small incisions were made: (i) on the lateral aspect of the hindlimb over the biceps femoris fascia; (ii) in between the scapulae. A subcutaneous tunnel created between these two incisions was used to lead the wires from the site of sensor implantation to a transcutaneous connector mounted on the back of the animal, in the region of the shoulder blades. After the skin was sutured, the animal was allowed to recover for two weeks prior to data collection. Additional doses of Buprenorphine were given 1-2 days after the surgery if signs of pain were noticed.

5.2.3 Data collection and analysis

Two weeks after sensor implantation, hindlimb kinematics, EMG activity and sonomicrometry crystals' distances were recorded during level and upslope (+20°) trotting. Only steady-state stride cycles were selected for further analysis, excluding galloping gaits and forward-backward acceleration on the belt (Sabatier et al., 2011). Data from 10-15s trials (30-50 stride cycles) were collected at a fixed treadmill speed of 0.6m/s, to obtain at least 15 stride cycles recorded with the rat trotting at a constant speed (Table 1). Only stride cycles satisfying these requirements were retained for further analysis of EMG and sonomicrometry data. For each animal, we pooled all stride cycles from all trials at a given slope to generate a single representative mean time series normalized to stride time for that animal and condition. EMG and sonomicrometry signals were sampled at 3120 Hz and digitized (Digital Sonomicrometer, Sonometrics, London, ON, Canada). Kinematic data and EMG-sonomicrometry signals from the implanted sensors were synchronized by an electronic trigger pulse to the sonomicrometry controller. Each measured variable was time-normalized to the stride-cycle time, and averaged first within and then across rats for the two different slopes.

5.2.4 Kinematics

Sagittal plane hindlimb kinematics were obtained from 2D videos during treadmill locomotion. The high-speed camera (A602f, Basler, Ahrensburg, Germany) was placed orthogonal to the treadmill, on the right side of the rat. Parallax errors were minimized by spatial transformation of the marker coordinates system with a calibration

checkboard and by using a narrow (11cm-wide) Plexiglas enclosed lane to limit medial-lateral movements on the treadmill. After shaving the right hindlimb, the following bony landmarks were marked using a permanent marker: the iliac crest, greater trochanter, lateral femoral epicondyle, lateral malleolus, 5th metatarsophalangeal (MTP) joint and the distal end of the 4th digit (Fig 5.1A, white circles). To minimize skin movements artifacts (Bauman and Chang, 2010), the position of the knee joint axis was triangulated based on the position of the greater trochanter and the lateral malleolus, and using the thigh and shank lengths. Video data (400x180 pixels, 7.4 pixel/mm) were sampled at 200 frames/s, streamed to an IEEE-1394 port and recorded to the computer hard drive with custom software (Labview, National Instruments Inc., Austin, TX).

Table 5.1 Animal characteristics, factors used for normalization and number of strides for each of the rats.

animal	*mass (g)*	*tibia length (mm)* *	L_{REF} *(mm)* **	*no. strides* +
1	273	37.5	7.5	32
			11.6	34
2	259	38.0	13.4	28
			16.7	19
3	297	40.0	8.6	26
			11.9	17
4	275	41.0	7.8	38
			8.5	16
5	260	37.0	9.9	20
			10.4	25
6	298	38.0	13.1	33
			11.2	22
7	281	40.0	7.5	26
			12.8	21

* normalization factor used for SO/LG MTU length

** normalization factor used for SO (upper value) and LG (lower value) muscle belly length

\+ upper value refers to level trotting, lower value refers to upslope trotting (+20°)

L_{REF}: reference length, defined as the mean of the maximum and minimum muscle belly lengths in swing during level trotting

Temporal stride characteristics and joint angles. A stride cycle was defined as the time between two toe-contacts of the same (right, implanted) hindlimb. For each stride cycle, the timing of two events was determined: i) the onset of the stance phase, defined as the video frame in which the foot of the hindlimb touched the treadmill belt (paw-in) and ii) the onset of the swing phase, defined as the video frame in

which the same foot left the ground completely (paw-off). The durations of stance and swing phases were calculated using the time points of these events. In addition, the stride length was calculated as the maximal absolute horizontal displacement of the toe marker during consecutive stance and swing phases. Angles of the hip, knee, ankle and MTP joints (Fig. 5.1A) were calculated based on the positional coordinates of the above described anatomical landmarks. In addition, the range of motion (ROM) for a given joint was calculated as the difference between the maximum and minimum angles during the stance and swing phases.

Muscle-tendon unit length. MTU lengths of LG muscle were estimated using the ankle-knee geometric model of the rat described by Ettema (1997). Inputs for the model were the low-pass filtered (third-order, zero-lag Butterworth, cut-off 20Hz) ankle-knee joint angles and the tibia lengths (see Table 5.1). In addition, displacements of the LG origin in response to changes in knee joint angle were calculated. The geometric model was adjusted to calculate MTU lengths of SO muscle using the SO origin on the tibia as measured after euthanasia.

5.2.5 Electromyography

EMG signals from SO and LG muscles (Fig. 5.1B) were amplified (100-2000x, CMRR>100dB), filtered for aliasing (10-1000Hz) and sampled (3120Hz). Band-pass and notch digital filters were subsequently applied to remove movement artifacts (30-1000Hz, third-order Butterworth) and power-line noise (50Hz, third-order Butterworth). The envelope of the filtered EMG signal was computed as the magnitude of the discrete-time analytic signal calculated by the Hilbert-transform, and subsequently time-normalized to 100 time bins per stride. For each rat, the amplitude of the EMG envelope for each time bin was normalized to the maximum EMG value across all time bins from all step cycles recorded during all conditions; this maximum was generally achieved in the upslope condition. The average EMG activity was then calculated as the mean of the normalized EMG envelope. The EMG data from one of the animals were excluded, because of insufficient signal-to-noise ratio. In addition to EMG amplitude, timing of EMG bursts was assessed using two descriptors: the absolute burst duration and the duration of the burst during the pre-stance phase. The onset-offset of muscle activity was determined by k-means cluster analysis applied on the band-pass filtered EMG signal (Den Otter et al., 2006), which corresponds to assigning values of the EMG amplitude to a user-defined number of clusters (n=3), with the lowest cluster reflecting inactivity. The range of MTU length changes was expressed as a percentage of the mean MTU length during the stride cycle.

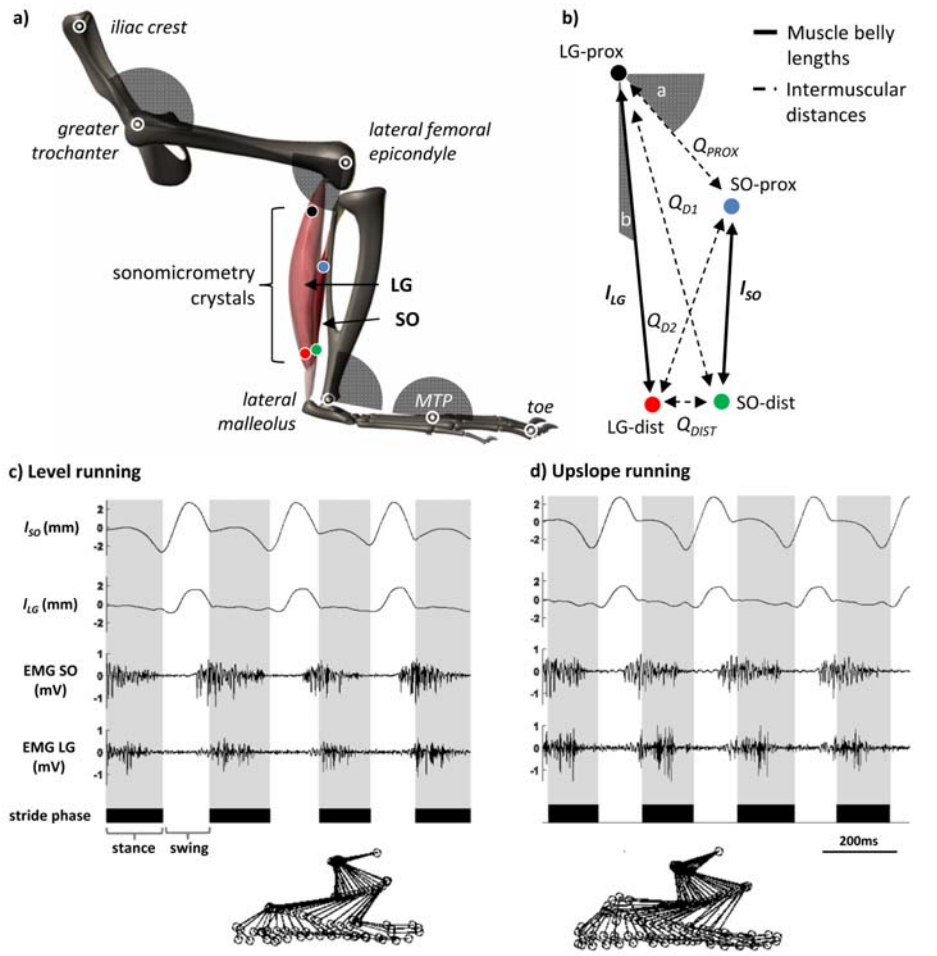

Fig. 5.1. *Overview of data collection.* Upper panel: a) 3D model of the rat hindlimb showing the motion tracking markers (white circles) on the selected anatomical landmarks and the convention for joint angular displacement (grey areas). The coloured dots indicate the position of the sonomicrometry crystals implanted in soleus (SO) and lateral gastrocnemius (LG) muscle bellies. b) Coplanar representation of the sonomicrometry crystals showing the nomenclature and position of the measured distances within and between the muscle bellies of SO and LG. α and β represent the difference between internal angles of the undeformed and the deformed-state. Lower panel: representative (from rat 1) muscle lengths patterns and raw electromyography (EMG) signals of SO and LG simultaneously recorded during 3 stride cycles of level treadmill trotting (c) and with a +20° slope (d), with an imposed speed of 0.6 m/s. Stance (dark grey areas) and swing (white areas) phases are highlighted based on the stride pattern of the right foot reported in the bottom axes. A 2D stick-diagram shows differences in the tracked hindlimb segments pattern during level (left) and upslope (right) trotting.

5.2.6 Sonomicrometry

Muscle belly length and velocity. The elapsed time for an ultrasound wave to be transmitted by one crystal and received by the other was used to assess the distance between two crystals, given the speed of sound at which the wave travels in vertebrate skeletal muscles (1580 m/s, Topp and O'Brien, 1999). Time series describing the muscle belly length changes of SO (l_{SO}) and LG (l_{LG}) during locomotion were low-pass filtered (second-order Butterworth, 50Hz cut-off). Values of l_{SO} and l_{LG} were normalized to the reference length (l_{REF}), defined as the mean of the maximum and minimum muscle belly lengths during the swing phase of level running (Gabaldón et al., 2004). Muscle belly velocity of length change of SO (l'_{SO}) and LG (l'_{LG}) was computed using the method of finite differences. Positive velocity values indicated lengthening, while negative values indicated shortening. The relative contraction velocity between SO and LG was calculated at each time bin as the difference l'_{SO} - l'_{LG}.

Tendon length. Tendon length (l_T) was estimated as the difference between MTU length (l_{MTU}) and muscle belly length:

$$l_T = l_{MTU} - (l_{norm} \cdot l_{belly}) \quad (1)$$

Where l_{norm} is the mean normalized distance between crystals (l_{SO}, l_{LG}) and l_{belly} is a reference measure of the whole muscle belly length (l_{belly}), including the proximal (l_{REF}^{prox}) and distal (l_{REF}^{dist}) regions of the muscle belly not comprised between the sonomicrometry crystals:

$$l_{belly} = l_{REF} + l_{REF}^{prox} + l_{REF}^{dist} \quad (2)$$

The length of these regions was measured for SO and LG in the euthanized animal after data collection. The length of SO and LG distal tendons (l_T^{dist}) was then calculated as follows:

$$l_T^{dist} = l_T \cdot (1 - \frac{T_{prox}}{T_{prox}+T_{dist}}) \quad (3)$$

Where T_{prox} and T_{dist} represent the reference length of the proximal and distal tendons, respectively. These were measured in previous experiments in our lab (Tijs & Maas, unpublished data) on animals with matching characteristics (Wistar male rats, mass ± SD: 321.8 ± 34.2, n=24). Distal tendon length changes were expressed relative to T_{dist}.

Intermuscular deformation. The measured distances between pairs of crystals implanted in the proximal and distal regions of either the SO or LG muscles provide information regarding the longitudinal and transversal intermuscular deformations. In a simplified coplanar representation, the four crystals form a quadrangle whose sides and diagonals lengths are known, since each piezoelectric transducer function both as a transmitter and as a receiver in respect to all the others (Fig. 5.1A). To assess muscle belly displacement between SO and LG, we measured the changes in length occurring between the proximal (Q_{PROX}) or distal (Q_{DIST}) intermuscular regions as well as changes in length of a major diagonal (Q_{D1}), from LG-proximal to SO-distal, and a minor diagonal (Q_{D2}), from SO-proximal to LG-distal (Fig 5.1B). All measured distances were expressed relative to the mean value measured over the whole stride cycle. A simple measure of deformation of such quadrangle was defined as the sum of the angles ($\alpha+\beta$), which represents the difference between internal angles of the undeformed and the deformed-state. Given that:

$$Q_{RATIO} = \frac{Q_{D1}}{Q_{D2}} = tan(\alpha + \beta) \quad (4)$$

the ratio between the major and minor diagonals was used as a comprehensive descriptor of 2D intermuscular deformation. This ratio was normalized to the mean value over stride.

5.2.7 Statistics

Paired-sample t-tests were performed to assess effects of slope condition on joint-angles, MTU length changes, stride characteristics and amplitude of SO and LG activity. For the following groups of similar outcome variables, p-values were Bonferroni corrected (p x n) for multiple comparisons (n): stance-swing duration and stride length (n=3), hip peak extension/flexion in stance and swing (n=4), MTP peak extension/flexion in stance and swing (n=4), Q_{RATIO} peak and range (n=2). Two-way repeated measures ANOVAs were performed to test for effects on timing of peak extension/flexion (independent factors 'slope' and 'joint'). Two-way repeated measures ANOVAs with independent factors 'slope' and 'muscle' were formed to test for effects on amplitude of SO and LG activity, on timing of muscle activation, tendon lengthening, muscle belly length and velocity. If significant interaction was found, post-hoc tests with Bonferroni correction were performed. Statistical tests were performed using SPSS (v. 21, SPSS Inc., Chicago, IL, USA). In all statistical analysis, results were considered to be significant when $p < .05$. Variability of descriptors is expressed as standard deviations (SD).

5.3 Results

5.3.1 Kinematics of level and upslope trotting

The time devoted to stance and swing was 0.16 ± 0.01s and 0.12 ± 0.01s (57.1% and 42.8% of the stride time), respectively, while stride length was 0.18 ± 0.01m. Changing the slope did not result in different spatio-temporal characteristics of locomotion (stance: p= .829, swing: p= .522, stride length: p= .788). Details on all statistical analyses are reported in Table 2.

During level trotting, ankle and knee joint patterns were characterized by a yield phase in early stance followed by joint extension in late stance. The timing of peak extension and flexion of these two joints differed. Peak knee extension in stance occurred 8.6 ± 3.6 ms earlier than peak ankle extension (p = .005). During swing, knee peak flexion was observed 22.4 ± 6.1 ms earlier than ankle peak flexion (p< .001) (Fig. 5.2 a-b). The hip joint angle extended from 60° to 104° during stance and flexed during swing. The MTP joint angle decreased towards a flexion peak at 116° during stance, then it started increasing before paw-off up to a maximum angle of 181° during swing.

During upslope trotting, hindlimb joint angles were very similar to those during level trotting (Fig. 5.2). The timing of maximum knee flexion during swing was different than that of the ankle joint (20.0 ms earlier, p< .001), but no differences in timing were found for peak extension (p= .116). Compared to the level trotting condition, significant changes were found in the hip and MTP ROMs. The hip joint angle range increased during stance phase (Fig. 5.2 a-e, peak extension: p= .050; peak flexion: p= .005), while the MTP joint angle range decreased in swing (Fig. 5.2 d-e, peak extension: p= .031, Fig. 5.2 d-e) for upslope compared to level trotting, respectively.

These data indicate that only small changes in kinematics were used to accommodate the slope difference. The different timing of maximum and minimum angles of knee and ankle joints will cause changes in relative position between the SO and LG MTUs (see below).

Table 2. Overview of statistical analysis

Test	*dependent variable*	*slope*	*joint*	*muscle*	*Statistic*	*p-value*
two-way ANOVA repeated	peak extension time	x			F (1,6) = 0.079	0.788
			x		F (1,6) = 18.247	0.005*
	peak flexion time	x			F (1,6) = 3.947	0.094
			x		F (1,6) = 277.941	<0.001*
	pre-stance activation (duration)	x			F (1,6) = 0.368	0.570
				x	F (1,6) = 14.265	0.013*
	muscle belly lengthening (stance)	x			F (1,6) = 16.531	0.010*
				x	F (1,6) = 11.087	0.021*
	muscle belly lengthening (swing)	x			F (1,6) = 1.607	0.261
				x	F (1,6) = 15.292	0.011*
	muscle belly shortening (pre-stance)	x			F (1,6) = 2.202	0.198
				x	F (1,6) = 84.094	<0.001*
	muscle belly shortening (stance)	x			F (1,6) = 0.751	0.426
				x	F (1,6) = 14.993	0.012*
	peak lengthening speed	x			F (1,6) = 0.087	0.778
				x	F (1,6) = 46.847	<0.001*
	peak shortening speed	x			F (1,6) = 0.041	0.847
				x	F (1,6) = 8.885	0.025*
	tendon lengthening	x			F (1,6) = 0.009	0.928
				x	F (1,6) = 108.224	<0.001*
	EMG burst duration	x			F (1,5) = 0.032	0.866
				x	F (1,5) = 0.371	0.569
	peak EMG (stance) time	x			F (1,5) = 0.046	0.838
				x	F (1,5) = 23.378	0.005*
paired t-test	stance duration	x			t (6,1) = 0.000	1.000
	swing duration	x			t (6,1) = 0.000	1.000
	stride length	x			t (6,1) = 0.000	1.000
	peak extension angle hip (stance)	x			t (6,1) = 1.440	0.200
	peak flexion angle hip (stance)	x			t (6,1) = 3.143	0.020*
	peak extension angle hip (swing)	x			t (6,1) = 0.988	0.336
	peak flexion angle hip	x			t (6,1) = 0.952	0.320

(swing)			
peak extension angle MTP (stance)	x	t (6,1) = 0.000	1.000
peak flexion angle MTP (stance)	x	t (6,1) = 0.161	0.612
peak extension angle MTP (swing)	x	t (6,1) = 1.561	0.124
peak flexion angle MTP (swing)	x	t (6,1) = 0.000	1.000
range MTU length changes - SO	x	t (6,1) = 0.485	0.645
range MTU length changes - LG	x	t (6,1) = 0.025	0.981
SO-LG differential lengthening	x	t (6,1) = -1.245	0.268
Q_{RATIO} peak (stance)	x	t (6,1) = 1.233	0.474
Q_{RATIO} range (stance)	x	t (6,1) = 1.311	0.258
EMG magnitude SO	x	t (5,1) = -0.471	0.657
EMG magnitude LG	x	t (5,1) = -2.734	0.041*

Within factors: slope (level, upslope trotting), joint (ankle, knee joints), muscle (soleus (SO), lateral gastrocnemius (LG))

MTP: 5th metatarsophalangeal joint

* p-value < 0.05

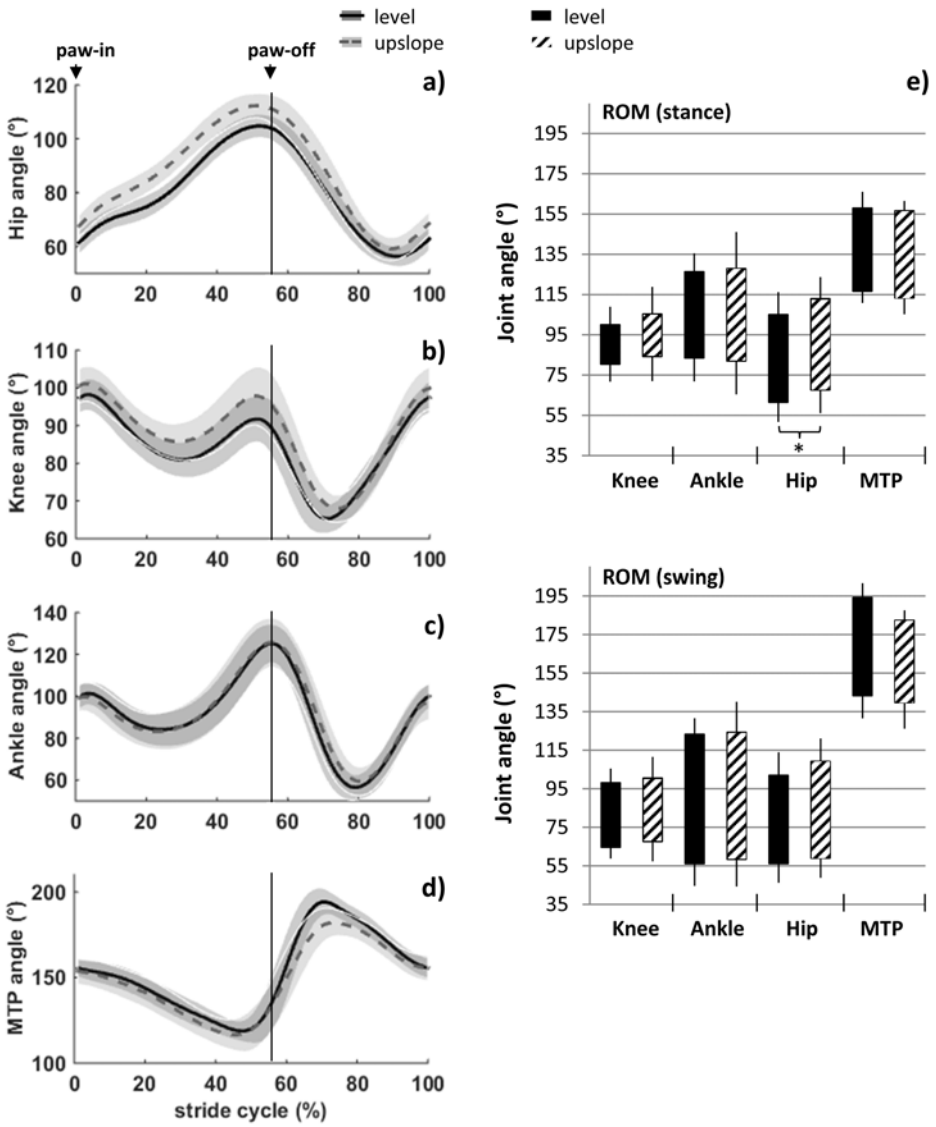

Fig. 5.2. *Hindlimb joint angles during treadmill trotting.* Sagittal plane hip (a), knee (b), ankle (c) and MTP (d) joint angles during level trotting (solid line) and upslope trotting (dashed line). Data (mean ± SD, n=7) are plotted as a function of normalized stride time. Treadmill speed was 0.6 m/s in all conditions and slope was 20°. Paw-off events occurred at 56.5 ± 1.1% of the stride cycle in both conditions (vertical line). e) Ranges of motion for each joint. Maximal (mean + SD) and minimal (mean - SD) joint angles during level trotting (black bar) and upslope trotting (striped bar). Asterisks indicates a significant difference in range of motion between level and upslope trotting ($p < .05$).

5.3.2 Activation patterns of ankle plantar-flexors during locomotion

During level trotting, the onset of activation for both SO and LG occurred in late swing (Fig. 5.3 A-B). Then, the activity of both plantar-flexors increased up to a peak during stance, which occurred earlier ($p < .005$) for SO than for LG (8.8 ± 3.7 ms and 47.6 ± 33.0 ms after paw-in respectively). Compared to LG, the SO showed a much steeper increase and decrease in EMG activity (Fig. 5.3A). The onset of SO activity was earlier than that of LG (Fig. 5.4C): the duration of pre-stance activation was higher in SO than in LG ($p = .024$, 0.05 ± 0.01s and 0.03 ± 0.01s, or 16.7 ± 4.5% and 10.7 ± 4.1% relative to stride duration, respectively).

Compared to level trotting, the EMG amplitude (Fig. 5.4A) increased substantially during upslope trotting in LG (by 53.6%, $p = .041$), but not in SO ($p = .657$). Total burst duration did not differ between level and upslope conditions (Fig. 5.4B). No difference in the duration of the pre-stance activation between SO and LG was found for the upslope condition ($p = .056$).

Overall, these patterns indicate co-activation of SO and LG, with SO onset preceding LG onset. Although they were largely active simultaneously, the pattern of activity was rather different between these synergistic muscles, suggesting differential contractile conditions.

5.3.3 Length changes of synergistic muscles during locomotion

During level trotting, LG showed only small length changes in stance phase, while SO muscle belly lengthened and shortened substantially (up to 15.8% of l_{REF}; $p = .012$; Fig. 5.3 c-d, Fig 5.4 d-e-g).. During swing, SO muscle lengthened by 33% of l_{REF}, while this was 21% for LG ($p = .004$). In addition, pre-stance shortening of SO was considerably larger than that of LG (30% and 13% of l_{REF}, respectively; Fig. 5.4 F; $p < .001$).

Peak lengthening velocities of SO and LG during swing were different (86.8 ± 22.5 mm/s and 39.6 ± 8.0 mm/s, respectively, $p = .001$) and the time point at which these occurred was slightly shifted between the two muscles (Fig. 5.5 A-B). This yielded a pattern of relative velocities between SO and LG muscle lengths with a peak of differential velocity in swing at 64% of the stride cycle, when SO starts shortening earlier than LG, resulting in a positive relative velocity of 55.9 mm/s for level trotting (Fig. 5.5C). An effect of slope was found only for muscle lengthening during stance (Fig. 4 e, $p = .010$). All the other measures of muscle lengths and velocities of SO and LG during contraction and relaxation did not significantly change between level and upslope locomotion (Fig. 4 d-f, g-h). Therefore, for most parameters only the data for

level locomotion were reported. These results indicate that changes in muscle relative positions and relative velocities are substantial at specific instances of the stride cycle.

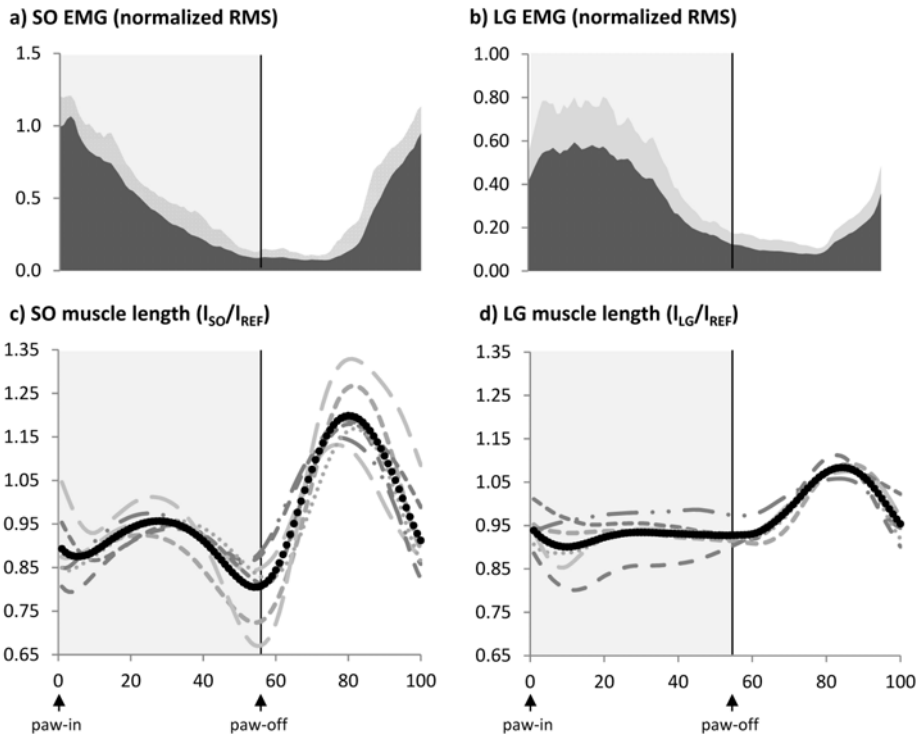

Fig. 5.3. *EMG activity and muscle belly length changes of SO and LG during level trotting.* The upper panel shows the filtered rectified EMG envelope of SO (a) and LG (b), normalized to the maximum amplitude measured for the upslope condition (n=6). The lower panel shows the muscle belly lengths l_{SO} of SO (c) and l_{LG} of LG (d) for each animal (n=7) and their mean pattern (black dots). l_{SO} and l_{LG} were normalized to the reference length of each muscle l_{REF}, defined as the mean of the maximum and minimum lengths in swing during level trotting. Normalized EMG envelopes and normalized muscle belly lengths are plotted as a function of normalized cycle time (% stride) during trotting on a level surface (mean + SD). The events of paw-in and paw-off are indicated in the bottom panel by arrows. The stance and swing phases are denoted by the grey shaded and white areas, respectively.

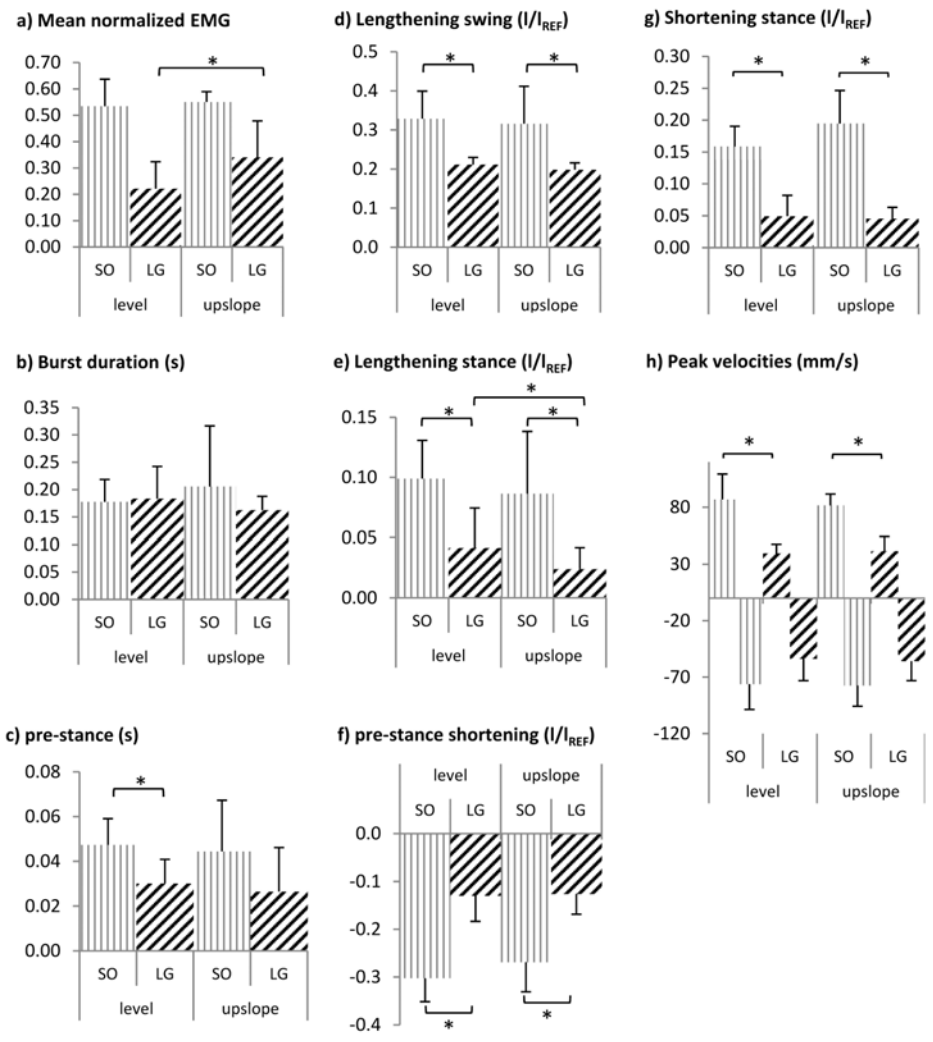

Fig. 5.4. *Comparison between level and upslope locomotion across animals.* Mean ± SD values (n=7) are presented for EMG bursts (left panels), contraction behaviour (central panels) and velocities of contraction (right panel) of SO and LG muscles. a) normalized mean EMG amplitude. b) burst duration, time from burst onset to cessation. c) pre-contact activation time. d-e) magnitude of lengthening during swing (d) and stance (e) phases. f-g) magnitude of shortening during pre-contact (f) and stance (g) phases. All length measures were normalized to reference length l_{REF}, defined as the mean of the maximum and minimum lengths in swing during level trotting. h) Maximal lengthening (positive) and shortening (negative) velocities during whole stride cycle. (*p< .05).

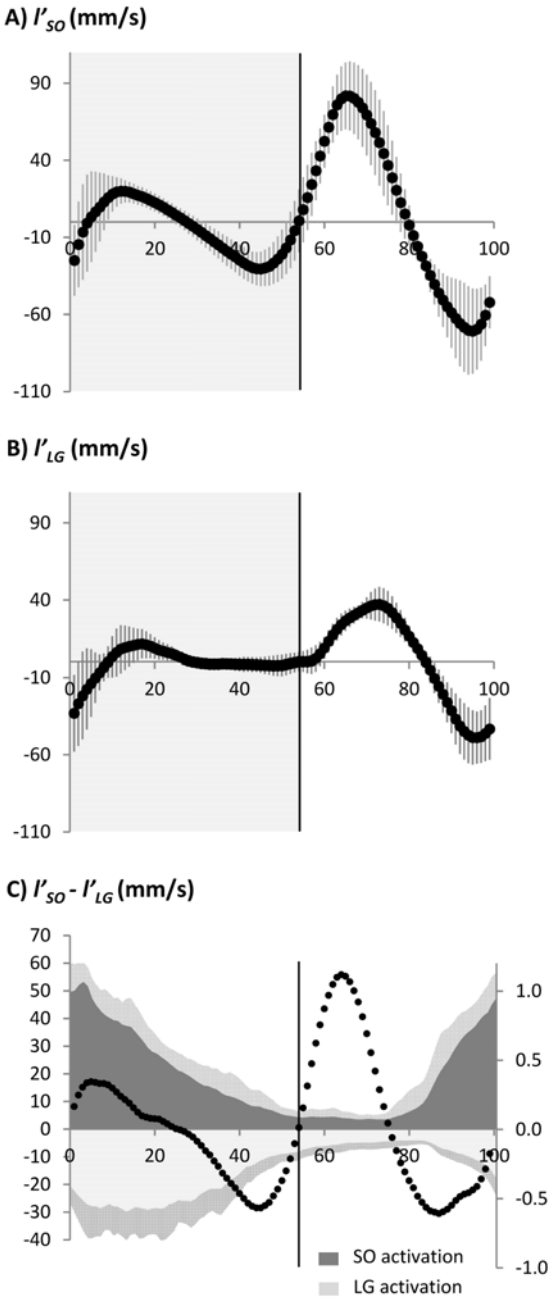

Fig. 5.5. *Individual muscle contraction velocity and relative velocity of SO and LG.* Averaged velocity of SO (a) and LG (b) muscle bellies plotted as a function of normalized cycle time (% stride) for the level trotting condition (n=7), error bars indicate SD. Stance and swing phases are highlighted by grey and white areas, respectively. Positive velocities correspond to muscle belly stretching, while negative velocities correspond to shortening. c) SO muscle belly velocity over stride is expressed relative to LG muscle belly velocity for level trotting. Simultaneously measured muscle activity expressed as normalized SO (dark grey) and LG (light grey, inverted) EMG envelopes were superimposed (secondary axis, n=6, mean + SD).

5.3.4 MTU length estimates and tendons differential lengthening

With combined knee and ankle angular displacement, the estimated MTU length varied between 29.3 and 35.7 mm for SO and between 37.6 and 44.9 mm for LG (corresponding to 19.8% and 17.6% of the average MTU length across the stride cycle for SO and LG, respectively; Fig. 5.6a). The LG MTU length changes caused by knee joint angular displacement only, i.e. proximal lengthening, were between 40.7 and 42.1 mm during level trotting, which corresponds to 3.4% of the average LG MTU length. This did not differ between level and upslope conditions (data not shown), as expected from kinematics data. These results shows that changes in LG MTU length were mainly determined by ankle joint angular displacement.

Estimates of distal tendon lengths of SO and LG showed that most of LG MTU length changes were the results of changes in tendon length, up to 3.1 mm during stance (7.5% of mean LG MTU length over the stride), but this was not the case for SO, the tendon of which lengthened by maximally 0.9 mm during stance (2.5% of mean SO MTU length, Fig. 5.6c). This is consistent with the rather isometric behavior of the muscle belly observed during stance for LG (Fig. 5.3d); resulting in differential lengthening, especially just before paw-in at 52% of stride cycle (1.9 mm or 4.7% of mean LG MTU) and in swing at 74% of stride (2.0 mm or 4.8% of LG MTU length) (Fig 5.6c). SO and LG tendons length changes and differential lengthening was not altered by the slope (2.0 and 1.6 mm in stance and swing, respectively; data not shown). Given that the distal SO and LG tendons merge into a common tendon, these results suggest unequal strain of Achilles tendon fascicles.

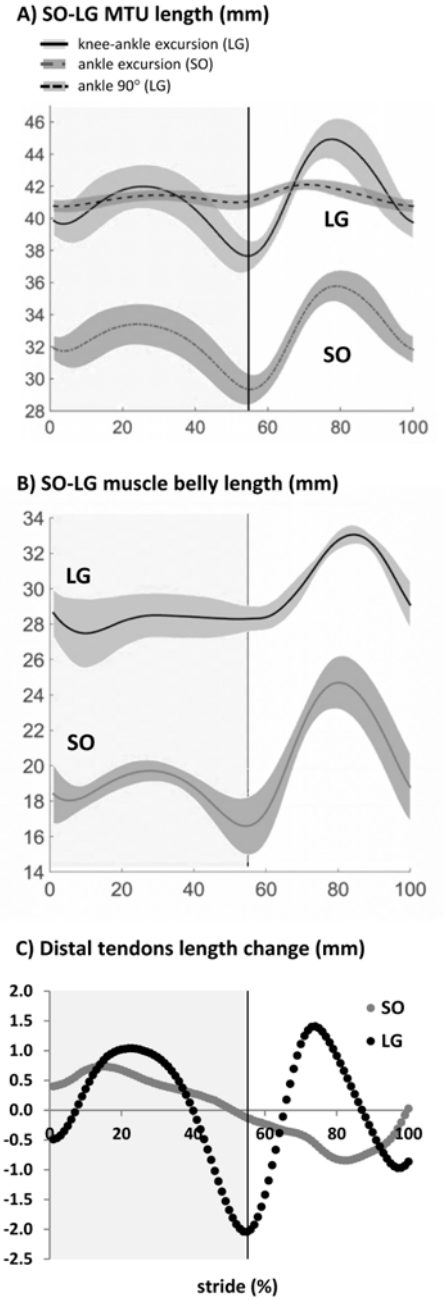

Fig. 5.6. *Estimates of MTU lengths and distal tendons lengths.*Mean (±SD, n=7) length of SO (grey line) and LG (black line) MTUs (a) and length of distal SO and LG muscle bellies (b) plotted as a function of normalized cycle time (% stride). MTU length of LG with knee joint angular displacement only and ankle angle fixed at 90° is also shown (black dashed line). c) Changes in length of the distal tendons of SO (grey) and LG (black). Stance: grey area; swing: white area.

5.3.5 Relative displacements

The maximum distance between sonomicrometry crystals (0.57mm relative to the mean) implanted in the proximal region (Fig. 5.7A) of SO and LG muscle bellies (Q_{PROX}) was found at 52% of the stride, i.e. at the end of stance phase, while a minimum (-0.74 mm relative to the mean) occurred at 78% of the stride, i.e. during swing. In contrast, the distance between sonomicrometry crystals implanted in the distal regions of SO and LG muscles (Q_{DIST}) did not show a consistent pattern that could be related to phases in the stride cycle. This distance varied maximally 0.37 mm (Fig. 5.7B). The major ($Q_{D1,}$ Fig 5.7C) and minor ($Q_{D2,}$ Fig. 5.7D) diagonals of the quadrangle defined by the four crystals are indicative of the quadrangle shape and were used to assess the shear deformation between SO and LG muscle bellies. Q_{D1} was nearly constant during stance, but increased during swing to a maximum of 1.24mm (relative to mean) observed at 85% of stride. Also for Q_{D2} the maximum of 1.50mm (relative to mean) was found at 80% of the stride. The different length patterns of the two diagonals caused changes in the shape of the quadrangle, which were represented by Q_{RATIO} (Fig. 5.7E). At paw-in, Q_{RATIO} reached its maximum (17.3%), to decrease to its minimum (-21.8%) at 80% of stride cycle (swing phase). Trotting upslope did not result in significant changes in the deformation pattern (Fig. 5.7E, lower panel: mean ± SD).

The similarity between patterns of Q_{D1} and Q_{D2} and those of LG and SO muscle belly lengths (see Fig. 5.3 C-D) suggests that the deformation of the intermuscular volume was determined by SO and LG contractile behaviour. These results indicate that both longitudinal and transversal deformations of intermuscular tissues would mainly be found in the proximal intermuscular region, while the distal muscle belly ends did shear relative to each other without much lengthening of connective tissues between the muscles at this location, as the distal distance was nearly constant with substantial changes in Q_{RATIO}.

Fig. 5.7. *Descriptors of relative displacement and deformation between synergistic muscles*. Left panel: SO and LG muscle bellies relative displacement plotted as a function of normalized cycle time (% stride). Reciprocal distances between sonomicrometry crystals implanted in SO and LG proximal (Q_{PROX}) and distal (Q_{DIST}) muscle belly regions were expressed relative to the mean value over a trial and averaged within and across animals (mean ± SD, n=7). Positive distances describe an increase of proximal (a) or distal (b) relative muscle position between SO and LG, while negative distances occur when muscle belly are moving towards each other beyond their mean distance. The four crystals form a quadrangle shape whose diagonals (c-d) show the shear deformation between SO and LG muscle bellies. (e) the ratio between the quadrangle diagonals (Q_{D1}/Q_{D2}) was normalized on the mean value for each animal and plot as a function of normalized cycle time (% stride) for level (black dots) and upslope (grey dots) locomotion (n=6, mean + SD). The EMG envelopes of SO (mean + SD, dark grey) and LG (mean + SD, inverted, light grey) are superimposed (n=6; secondary axis). RMS values were normalized to the maximum amplitude measured during upslope trotting. Lower panels in (e) show a 2D geometrical representation of the quadrangle shape at the time of paw-in,

paw-off and at 80% of the normalized stride cycle, when maxima and minimum Q_{RATIO} occurred. Left (LG) and right (SO) solid red lines represent muscle belly lengths, while the black thin lines describe the proximal and distal intermuscular distances (Q_{PROX}, Q_{DIST}) according to data in a-b plots.

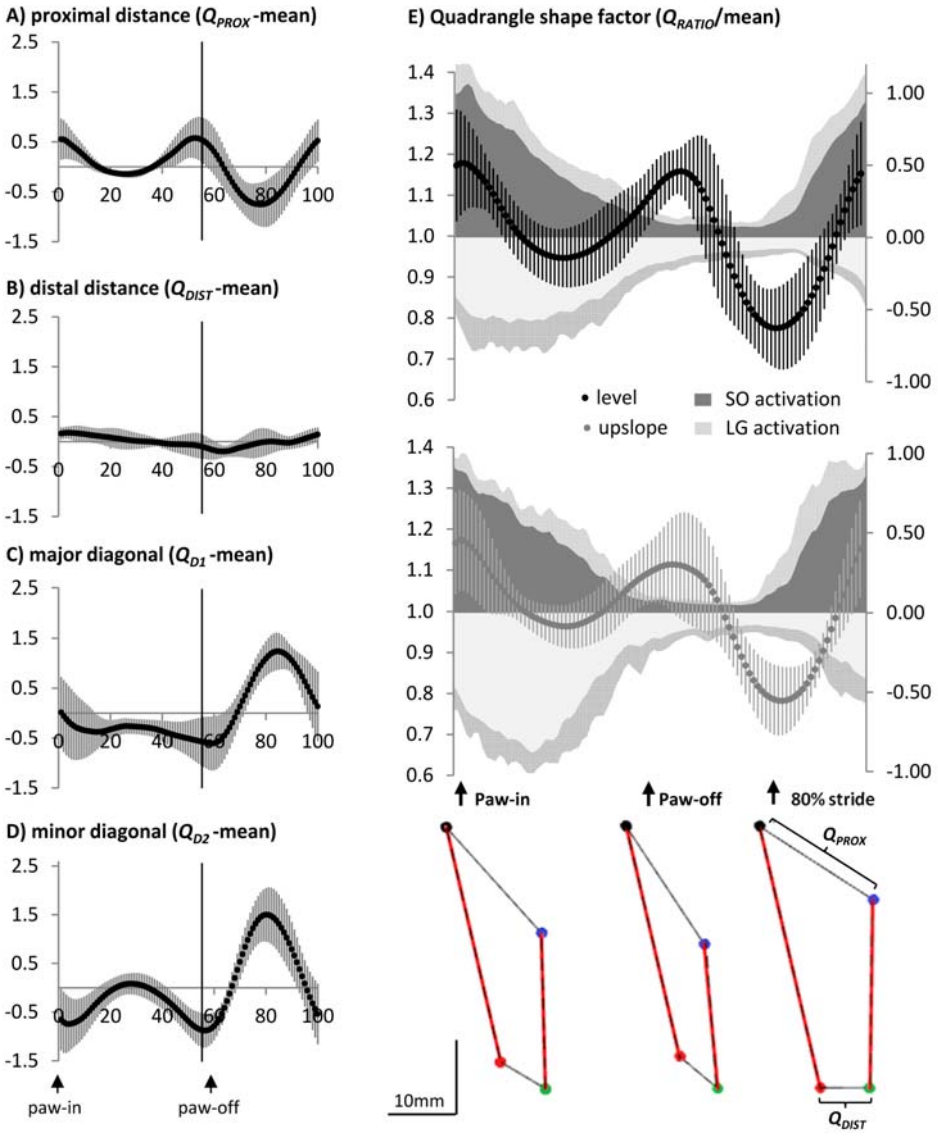

5.4 Discussion

Adjacent muscles with different functional roles can exhibit substantial differences in their pattern of activation and contractile behavior, especially in a multi-joint muscle system such as the ankle-plantar flexor group. Mechanical interaction between these muscles via common tendons and connective tissues at their shared interface may affect force and strain distribution among the individual actuators. For understanding how these muscles are controlled and how they eventually deliver force at the joints spanned requires detailed knowledge about the coordinated action of muscle groups. This is the first study providing a measure of the deformation of the intermuscular volume between two adjacent muscles during locomotion. We confirmed that the different functional role of SO and LG requires these muscles to undergo differential length changes, despite the fact that they merge in a common tendon distally. We observed displacements between the SO and LG muscles during locomotion, which may have implication for intermuscular force transmission. In contrast to our expectations, the extent of muscle relative displacement was not substantially affected by the imposed increase in the slope of the treadmill. Differential changes in muscle belly lengths and relative velocities of SO and LG were likely the result of non-simultaneous muscle activation. The relative displacements and activation levels of the muscles studied were those occurring in the freely moving animal, thus providing information about the extent of mechanical and functional interaction between muscles in an intact environment and with physiological muscle recruitment. Differential action of synergistic muscles has been observed in several species with a similar approach (Biewener et al., 1998; Daley, 2003; Ellerby and Marsh, 2010; Higham et al., 2008; Maas et al., 2009).

5.4.1 Heterogeneity of contraction behaviour and muscle activation between ankle plantar-flexors

We found substantial differences in length changes and muscle activation between SO and LG muscles of the rat. By active lengthening during the stance phase, the SO muscle belly likely contributed to negative work absorbing the body inertial load after paw-in. In contrast, the almost isometric behaviour of the LG suggests that this muscle stored elastic energy in its tendon (Griffiths, 1991)**.** These data indicate a potential difference in the timing and the amount of energy absorbed by the two muscle bellies during active lengthening. Although frequently co-activated, the timing of EMG bursts between these muscles was rather asynchronous, with the SO onset of activation occurring earlier during pre-stance than that of LG. In addition, only the EMG amplitude of LG increased substantially during upslope trotting (by 54%) while no

changes were observed in SO. Heterogeneity of muscle lengths and velocity between synergists during contraction may be explained by such differences in the neural drive, but also by architectural properties, such as pennation angle and fibre type composition (Armstrong and Phelps, 1984). Previous studies have shown that muscle activation and muscle fascicle deformation differ between ankle plantar-flexors (Cronin et al., 2013; Maas et al., 2009). Also, the force produced by ankle plantar-flexors and their contractile behaviour has been reported to be quite diverse (Daley, 2003; Prilutsky et al., 1996). In humans for instance, asynchronous shortening of SO and LG during the limb extension phase of jumping allows LG to store the power produced by the knee extensors in the series elastic element at the ankle, acting in a strut-like manner (Bobbert et al., 1986; Farris et al., 2016). It is conceivable that architectural diversity together with a fine-tuned neural drive, allows for adaptation to varying constraints, e.g. different locomotor speeds and motor tasks (Gillis and Biewener, 2001; Gregor et al., 2006; Hodson-Tole and Wakeling, 2008; Hutchison et al., 1989), as suggested also by the different responses in EMG amplitude to changes in slope between LG and SO reported here.

Although different activation and contractile behavior for two muscles arranged in parallel and merging in a common tendon may seem paradoxical, such diversity may constitute a key feature for flexibility, subserving the rat's behavioral repertoire. The rat triceps surae allows both damping and energy recoil: while SO absorbed energy by deformation, LG responded more isometrically for storing energy in its tendon during gait. In addition, only the activation of the LG muscle was modified in response to environmental changes (slope). This suggests that by selectively activating one muscle in the synergistic muscle group, its specific mechanical response can be exploited. In more specialized animals, the anatomy appears more tuned to just one of these functions. For instance, plantaris (PL) and LG muscles fuse for much of their length in the possum (*Trichosurus vulpecula*), forming one functional unit, while the SO is absent (Hore and Porter, 1972). In the camel (*Camelus dromedarius*), plantaris muscle fibers are vestigial, replaced by a long tendon (Alexander et al., 1982). Likewise, in the horse (*Equus caballus*) the digital flexor muscles have extremely short muscle fibers with very long tendons spanning several joints (Wilson et al., 2001). In other species, energy storing efficiency is maximized by shortening or removing muscle fibers (for a comparison, see Biewener and Roberts, 2000). These observations on specific mammals suggest that evolutionary changes of the triceps surae architecture would have involved separation or fusion of a previously present and functionally unsuitable set of muscles.

5.4.2 Mechanical consequences of displacements between neighbouring muscles

Our data indicate that displacements and velocities between neighbouring muscle bellies can be substantial in the freely moving animal. We found the displacement between SO and LG to be maximal in the proximal region (Q_{PROX}), consistent with the location of their origins on the skeleton. In fact, the distance between SO and LG is expected to increase proximally with knee extension, as SO and LG are set apart because of their independent origin and because LG spans the knee joint and SO does not. Moreover, substantial changes of the quadrangle shape at paw-in and during swing (+17.3% and -21.7% relative to the mean diagonals' ratio) indicate that intermuscular displacement does not occur only in one dimension, but that it is rather a combination of longitudinal and transversal displacements. As a consequence of different shape changes of neighbouring muscles due to variation in pennation angles (Azizi and Roberts, 2014) and relative muscle belly length changes in response to muscle excitation, deformation of the intermuscular volume must occur. Knee-ankle joint coordination and subsequent changes of orientation between one- and two-joint muscles' lines of pull also cause deformations of the intermuscular volume. It has been shown that changes in relative position of neighbouring muscles affect epimuscular myofascial force transmission (Huijing and Baan, 2003; Maas et al., 2003). Several structures are present in the intermuscular volume between ankle plantar-flexors and, with substantial relative displacements, likely change their tensional state, possibly modifying force transmission between SO and LG. Connective tissues are found across the whole surface between SO and LG muscle bellies, with the neurovascular tract running centrally between SO and LG muscle bellies (Fig. 5.8 a; see Bernabei et al. 2016 for a detailed description). Bundles of connective tissues surrounding blood vessels and nerves reaching the posterior crural muscles can be divided in two main force transmission pathways. The first pathway runs from the proximal-ventral side of LG to the dorsal side of SO. The second pathway contains branches of the popliteal artery and tibial nerve running from the popliteal fossa to the proximal-dorsal surface of lateral and medial gastrocnemius muscle bellies. *In situ*, mechanical interaction between SO and LG of the rat has been reported (Bernabei et al., 2015) for a range of MTU lengths (6 mm), which were consistent with the ones estimated in this study (7.2 and 6.4 mm for LG and SO, respectively; Fig. 5.6a). However, in the latter study both muscles were maximally activated, while the extent of mechanical interaction has been shown to decrease with submaximal activation and passive muscle conditions (Tijs et al., 2015a; Tijs et al., 2016a). Moreover, the maximal MTU relative displacement imposed in the study by Bernabei et al. (2015) was larger (3.0 mm) than that found *in vivo* in the present study (1.4 mm). It should also be noted that in previous experiments only one-dimensional (longitudinal) relative displacements

between muscle-tendon units were imposed. However, we found here that an increase in longitudinal relative position was accompanied by a decrease in orthogonal intermuscular distance (Fig. 5.7e), thereby reducing the strain of the intermuscular connective tissues. This could partially explain the limited or no mechanical interaction between muscles when intact muscle compartments and physiological joint excursions in rats and cats hindlimb muscles were tested (Sandercock and Maas, 2009; Tijs et al., 2015b). According to previous studies relating the amount of intermuscularly transmitted force with active and passive state of muscles (Bernabei et al., 2016a; Tijs et al., 2016b), the largest effects of intermuscular force transmission are expected during the pre-stance and stance phases, when both LG and SO are active. When the relative position changes between passive muscles, compliant intramuscular structures will likely fully absorb the resulting shear strain and, hence, the strain on intermuscular connections will be minimal. Therefore, the largest displacement and differential velocity of muscle belly observed during mid-swing likely involves negligible amounts of intermuscularly transmitted forces.

Our observed relative displacements and the previously reported minimal mechanical interaction between submaximally activated muscles suggest that during level and upslope trotting the extent of epimuscular force transmission between ankle plantar flexors is not significant in healthy rats. This may change in pathological conditions of the musculoskeletal system, such as those caused by muscle injury and surgical interventions, for which enhanced mechanical interactions between muscles have been reported (Bernabei et al., 2016a; Maas and Huijing, 2012).

5.4.3 The role of the common Achilles tendon

We estimated the difference in length changes between SO and LG distal tendons during locomotion to be maximally 4.8% of the mean LG MTU length. In contrast, we showed that the distance between the distal regions of SO and LG muscle bellies (Q_{DIST}) did not undergo substantial changes over the stride cycle. This could be explained by a stiff intertendinous connection between SO and LG tendons, which causes transversal displacement during longitudinal displacements (see Fig. 5.8 c-e). In the rat, the Achilles tendon can be divided in a proximal portion with separated tendon bundles from SO, LG and MG and a distal portion in which these bundles are fused together and no longer separable without dissection of connective tissues (Fig. 5.8 b). The total length of the tendon is about 10 to 15mm in an adult rat (male Sprague-Dawley, 400-425g; Krapft et al., 2012). A recent study reported that the length of the merged distal portion (about 45% of the total Achilles tendon length) can change from 6.6 to 6.9 mm depending on knee extension and activation of SO+GA or SO only (Tijs et al. 2015b,

male Wistar rat 315-340g). Only a few studies have assessed the mechanical responses of common tendon of the SO and LG in physiological conditions (Finni et al., 1998; Franz et al., 2015; Slane and Thelen, 2014). Interestingly, the consistent finding that the Achilles tendon fascicles in series with SO or LG undergo differential displacements was interpreted rather differently (Arndt et al., 1999; Bojsen-Moller and Magnusson, 2015). On one hand, this relative sliding may indicate that individual muscles transmit their forces independently; on the other hand, relative sliding may result in intertendinous force transmission. With regard to the latter, it has recently been shown that the matrix between tendon fascicles of equine tendons has elastic properties (Thorpe et al., 2012; Thorpe et al., 2015). This implies that forces can be transmitted between different tendon fascicles when substantial sliding occurs. Connective tissue linkages between tendons could serve as a stress-release mechanism protecting tendon fibres from damage by redistributing forces to neighbouring fascicles. Moreover, tendon bundles from the different muscles of the triceps surae could cooperate for elastic recoil as a system of elements arranged in a parallel fashion. An example of optimization of this mechanism for elastic recoil is given by the complex system of accessory ligaments in the horse lower limb (Wilson et al., 2001). Non-linear summation of joint moments of the triceps surae muscles found in the rat indicates that SO and LG tendons are not mechanically independent (Tijs et al., 2014b) and, hence, stress distribution seems likely. However, the function and implications of the complex arrangement of the triceps surae muscle-tendon unit remain not fully understood (Bojsen-Moller and Magnusson, 2015).

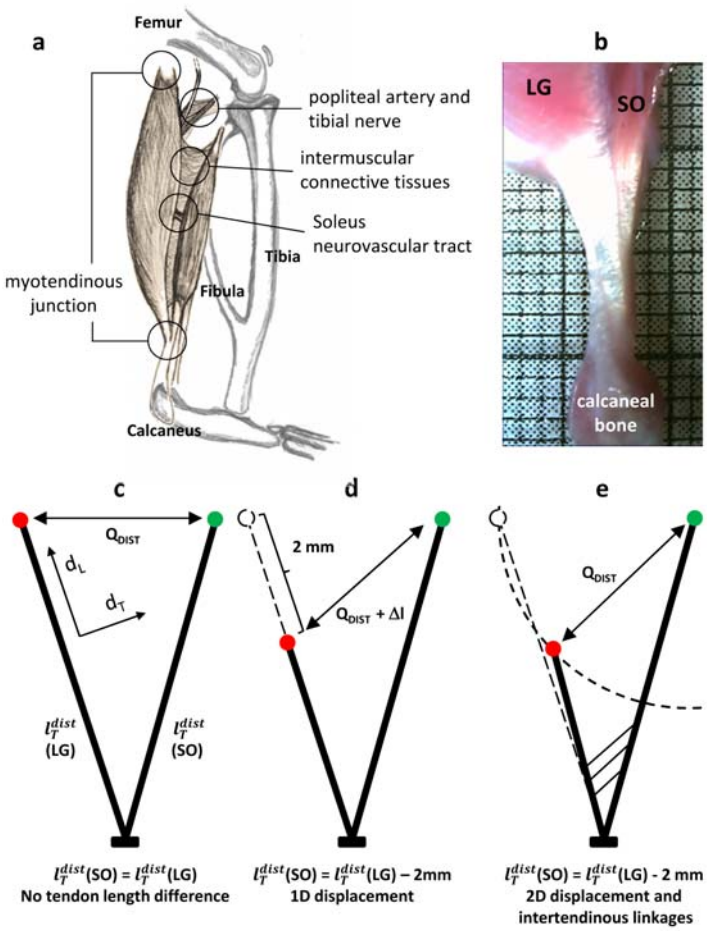

Fig. 5.8. *Force transmission pathways involving soleus and lateral gastrocnemius and 2D interaction between SO and LG distal tendons.* a) Drawing of the intermuscular linkages which connect lateral gastrocnemius (LG) and soleus (SO) muscle bellies. LG proximal tendon is detached from its origin on the lateral epicondyle of the femur to show the intermuscular connective tissues and SO muscle belly lying more anterior in the triceps surae compartment. Connective tissues surrounding blood vessels and nerves (i.e. the neurovascular tract) running to SO and LG connect these muscles to surrounding non-muscular structures. b) Photo of rat Achilles tendon (lateral view). The individual tendons of soleus and lateral/medial gastrocnemius are distinct in the proximal portion of the tendon, but merge distally. c-e) Schematic representation of the interaction between SO and LG tendon bundles within the Achilles tendon. Red and green dots represent the sonomicrometry crystals in the LG and SO muscle bellies; both distal tendons insert in the tuber calcanei, here approximated as a unique insertion point. We estimated a maximum of 2mm sliding between these two tendons, which would require an increase or decrease in length (⍁*l*) of the distance between the crystals (Q_{DIST}) when considering 1-dimensional displacement only (d_L). When 2-dimensional displacement is considered (d_L, d_T), stiff intertendinous connection between SO and LG tendons will cause transversal displacement (d_T). Such mechanical constraint could explain the little changes observed in Q_{DIST} with substantial SO and LG tendon sliding.

5.4.4 Limitations

Coordinated activation and contractile behaviour of two ankle-plantar flexors reported in this study were directly measured by implanted sensors, while MTU and tendon length changes were estimated. As a consequence, several issues needs to be considered when interpreting the results presented here.

i. It should be noted that MG is also part of the triceps surae muscle group and it shares an aponeurosis with the LG distally. However, in this study we focused on SO-LG interaction exclusively for several reasons. First, while there is evidence of direct connective tissues linkages between SO and LG muscle bellies (Fig. 8a), MG and SO do not share an interface. Second, previous studies have quantified the force transmitted via inter- and extramuscular connective tissues between SO and LG as a function of relative displacement (Bernabei et al., 2015; Bernabei et al., 2016b), while this information is not available for the LG-MG or SO-MG interaction. Third, we reduced the number of implanted sensors to minimize any effects on the muscle and connective tissues in response to implantation surgery. As a consequence, the present data do not allow us to draw conclusions regarding the interactions with MG.

ii. 2D data obtained from X-ray motion tracking and bone-derived markers (Bauman and Chang, 2010) yielded similar patterns of hind limb joint angular displacements on the sagittal plane. However, a biplanar motion tracking system is preferable to describe joint flexion-extension angles in 3D space if out-of-plane motion is substantial. Comparison between 2D vs 3D motion data of joint angular displacement revealed that large differences are found in the frontal and horizontal planes (Joãoa et al., 2010), while hip-knee-ankle flexion-extension during gait can be well approximated by motion on the sagittal plane.

iii. Use of 2D instead of 3D motion data limits the accuracy of the kinematic descriptors and the estimates of MTU lengths presented here. Based on previously reported 3D kinematics of the rat hindlimb (Thota et al., 2005) collected during walking at 0.3 m/s (NB. not trotting; much slower speed than in our experiment), we estimated a maximum projection error of 17.9° and 17.5° for knee and ankle joint angle changes, respectively. This discrepancy results in a maximum underestimation of 5.4% and 3.4% of the average SO and LG MTU length, respectively.

iv. Sonomicrometry crystals were implanted to measure relative displacement between muscle bellies and differential muscle belly strain. Due to the fact that LG is a pennated muscle, muscle belly length changes do not fully reflect the length changes of muscle fibers.

v. The assessment of distal tendon length changes could have been affected by out of plane (sagittal) movements of SO and LG muscle bellies. Due to projection errors, this would yield an overestimation of distal tendon lengths, especially during the swing phase and for LG muscle, because the sonomicrometry crystal distance vector may not be in the line of pull of the LG muscle belly and tendon. Also, 2D/3D motion data discrepancy (see iii) may influence this estimate, as modeled MTU lengths were used. Therefore, the estimated tendon length changes during swing should be interpreted with caution. More research is required to obtain accurate predictions of tendon forces from estimated tendon lengths.

5.4.5 Conclusion

This study provides evidence of differential muscle activation and contractile behaviour between rat plantar-flexors. We observed substantial longitudinal and transversal displacements between muscle bellies and subsequent deformation of the intermuscular volume. Such conditions may affect transmission of force between neighbouring muscles via epimuscular myofascial pathways and/or intertendinous pathways, but knowledge about the stiffness of these pathways is required to predict the exact magnitude of the resultant mechanical interaction. Studying not only the contractile behaviour of individual muscles, but also the multi-dimensional deformations between them, provides a more comprehensive view of the mechanical interactions within a synergistic muscle group and may be needed to fully understand neural control of movement.